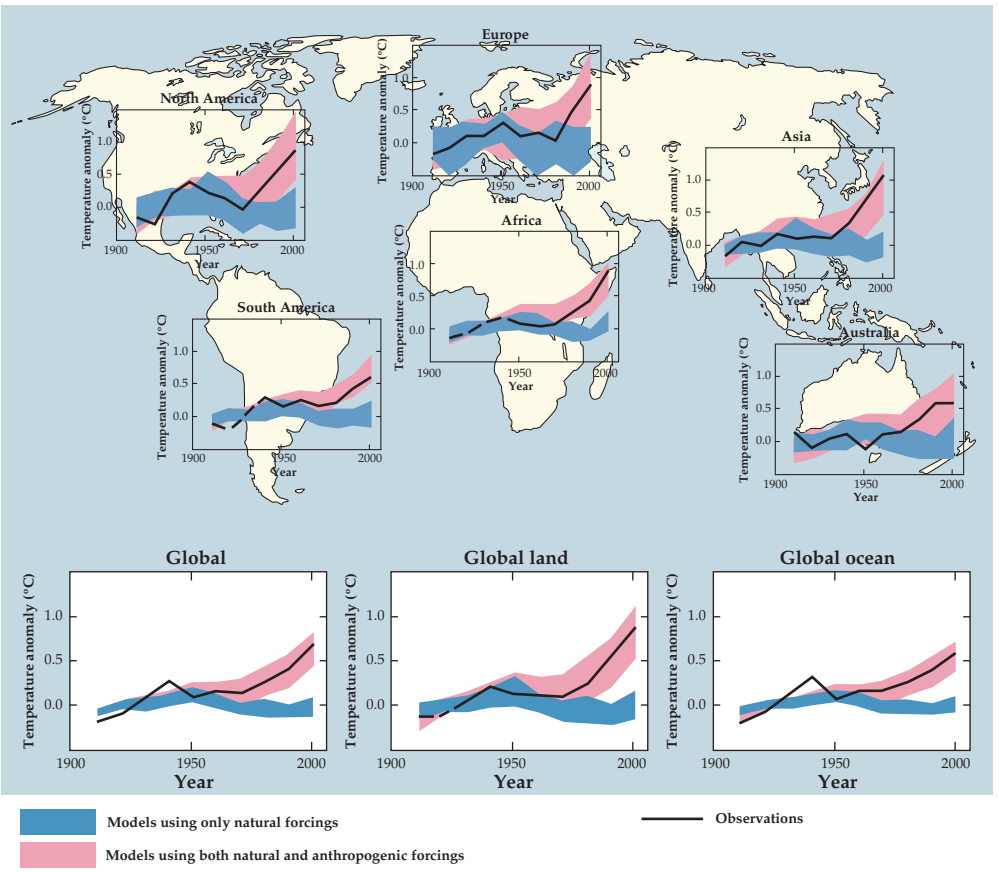

Plate 1 Comparison of observed continental- and global-scale changes in surface temperature with results simulated by climate models using natural and anthropogenic forcings. Decadal averages of observations are shown for 1906–2005 (black line) plotted against the centre of the decade and relative to the corresponding average for 1901–1950. Lines are dashed where spatial coverage is less than 50%. Blue shaded bands show the 5–95% range for 19 simulations from five climate models using only the natural forcings due to solar activity and volcanoes. Red shaded bands show the 5–95% range for 58 simulations from 14 climate models using both natural and anthropogenic forcings. The figure is taken from the Fourth Assessment Report of the Intergovernmental Panel on Climate Change WGI (Work Group I) Summary for Policymakers (IPCC, 2007a). See Figure 2.2, page 12.

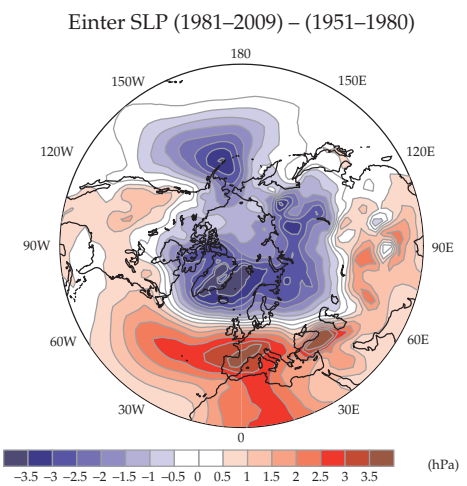

Plate 2 Boreal winter (December–March) average Northern Hemisphere sea level pressure (SLP) anomalies (hPa) since 1981 expressed as departures from the 1951–1980 average values. The SLP data are from Trenberth and Paolino (1980). See Figure 2.3, page 16.

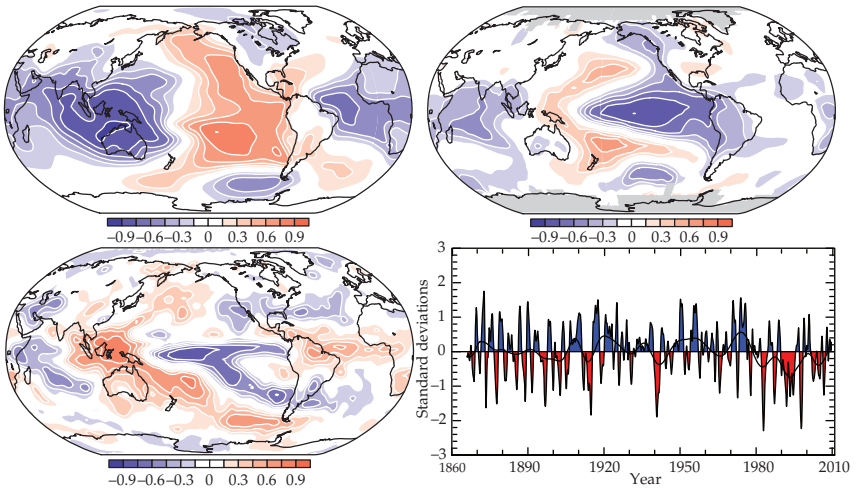

Plate 3 Correlations with the Southern Oscillation index (SOI) (Table 2.1) for annual (May–April) means for sea level pressures (SLP; top left) and surface temperature (top right) for 1958–2004, and estimates of global precipitation for 1979–2003 (bottom left), updated from Trenberth and Caron (2000) and IPCC (2007a). The Darwin-based SOI, in normalized units of standard deviation, from 1866 to 2009 (lower right) features monthly values with an 11-point low-pass filter, which effectively removes fluctuations with periods of less than 8 months. The smooth black curve shows decadal variations. Red values indicate positive SLP anomalies at Darwin and thus El Niño conditions. See Figure 2.5, page 19.

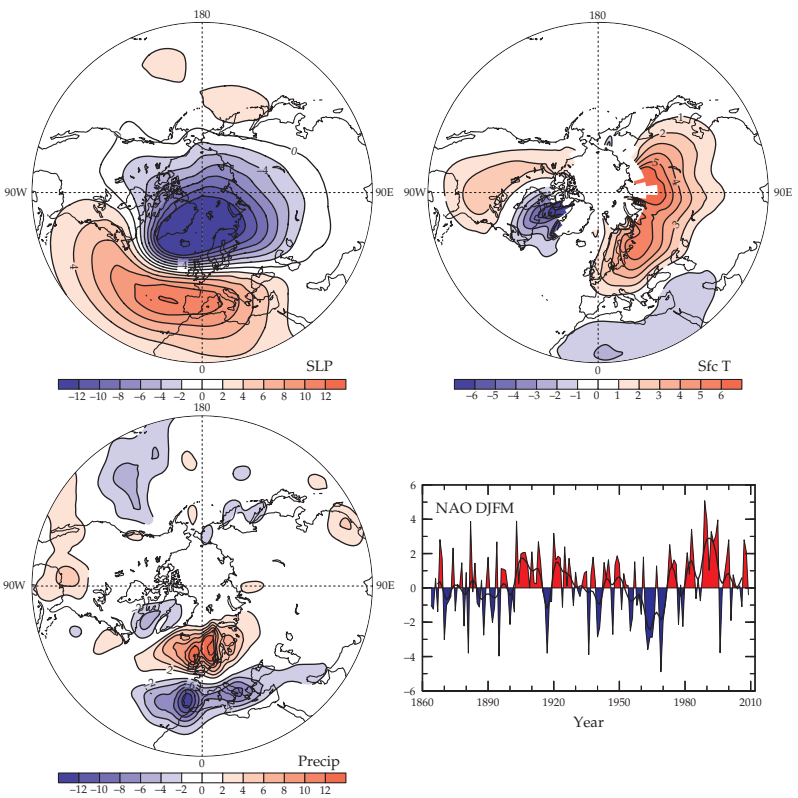

Plate 4 Changes in winter (December–March) surface pressure, temperature and precipitation corresponding to a unit deviation of the North Atlantic Oscillation (NAO) index over 1900–2009. Top left: Mean sea level pressure (0.1hPa). Top right: Land surface air and SST (0.1°C; contour increment 0.2°C): regions of insufficient data (e.g. over much of the Arctic) are not contoured. Bottom left: Precipitation for 1979–2009 based on global estimates (0.1mm/day; contour interval 0.6mm/day). Bottom right: Station-based index of winter NAO (Table 2.1). The heavy solid line represents the index smoothed to remove fluctuations with periods less than 4 years. The indicated year corresponds to the January of the winter season (e.g. 1990 is the winter of 1989/1990). Adapted and updated from Hurrell *et al.* (2003) and IPCC (2007a). SLP, sea level pressure; Sfc T, surface temperature; Precip, precipitation; NAO, North Atlantic Oscillation;DJFM, December, January, February, March. See Figure 2.8, page 23.

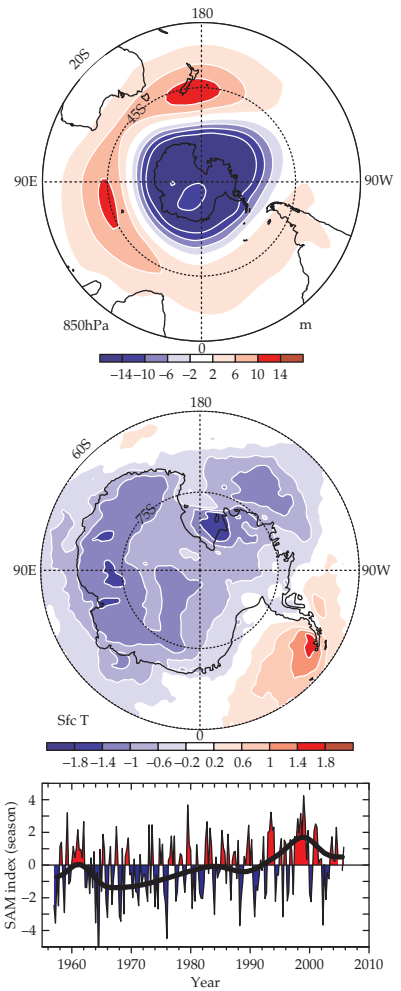

Plate 5 Bottom: Seasonal values of the southern annular mode (SAM) index (Table 2.1; updated from Marshall, 2003). The smooth black curve shows decadal variations. Top: The SAM geopotential height pattern as a regression based on the SAM time series for seasonal anomalies at 850 hPa (see also Thompson and Wallace, 2000). (Middle) The regression of changes in surface temperature (°C) over the 23-year period (1982–2004) corresponding to a unit change in the SAM index, plotted south of 60°S. Values exceeding about 0.4°C in magnitude are significant at the 1% significance level. Adapted from IPCC (2007a). Sfc T, surface temperature. See Figure 2.9, page 25.

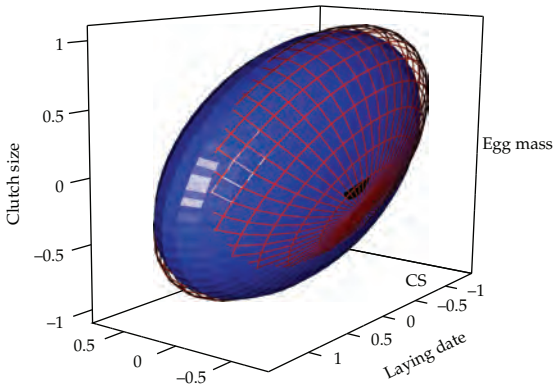

Plate 6 Visualization of the genetic variance–covariance matrix for three reproductive traits (laying date, clutch size, egg weight) in female great tits at Wytham, UK, estimated under two time periods with contrasting trends in early spring temperature: 1965–1988 (no warming trend) and 1989–2004 (rapid increase in early spring temperature). Each ellipsoid represents the genetic variance and covariance for the three traits in each time period: the filled surface represents the years when warming occurred and the wire-framed surface the years with no warming trend. The ellipsoids can be thought of as bounding a space containing 95% of the expected breeding values in a hypothetical population. As the volumes largely overlap, there is little evidence that genetic variance and covariance for these characters changed as the environment changed. Reproduced, with permission, from Garant *et al.* (2008). See Figure 12.2, page 156.

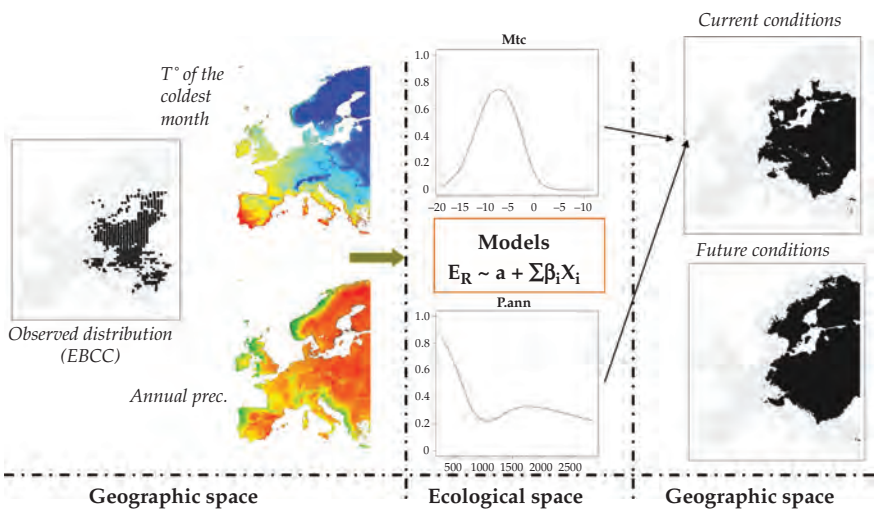

Plate 7 Diagram representing the concept of habitat suitability modelling. The observed distribution of a given species (e.g. from the European Bird Census Council atlas of European breeding birds, their distribution, and abundance) is related to relevant environmental data (e.g. climatic such as temperature (T°) of the coldest month and annual precipitation) using a statistical model (e.g. generalized additive model). Then, the niche of the species is projected back onto the geographic space to depict the potential current distribution (i.e. under current conditions) and the future potential suitable habitat (i.e. under future conditions). See Figure 8.1, page 78.

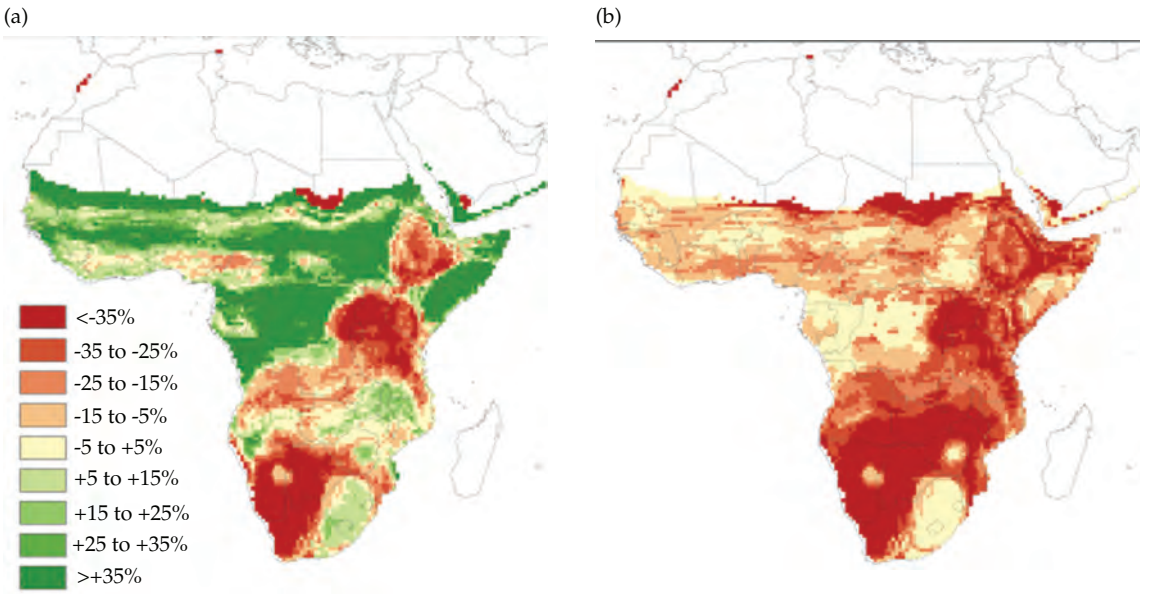

Plate 8 Predicted changes in species richness of migrant passerines in Africa under future climatic scenarios (by 2100). (a) Future-predicted variations in species' richness under the hypothesis of full dispersal ability between predicted present and future ranges and (b) future-predicted variations in species richness under the hypothesis of null dispersal ability. Based on Barbet-Massin *et al.* (2009). See Figure 18.1, page 280.

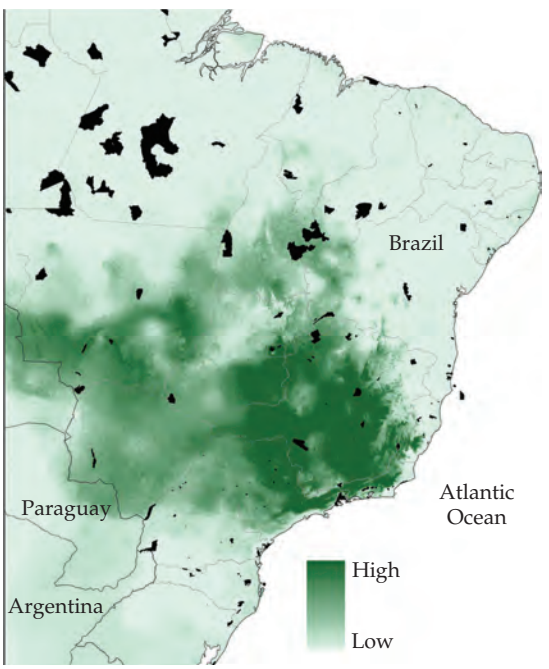

Plate 9 Predicted cumulative probabilities of occurrence for the 38 Cerrado birds in Brazil for the future (2046–2060), as obtained with an ensemble-forecasting approach. The colours in the maps represent the cumulative probability of occurrence (climatic suitability) within a pixel, ranging from 0 to 1 (pale to dark green). Large (>30,000ha) reserves are represented by black polygons. Based on Marini *et al.* (2009). See Figure 18.2, page 281.